Eur. Phys. J. B **60**, 469–476 (2007)
DOI: 10.1140/epjb/e2008-00018-0

THE EUROPEAN PHYSICAL JOURNAL B

Polymer and surface roughness effects on the drag crisis for falling spheres

N. Lyotard[1], W.L. Shew[1], L. Bocquet[2], and J.-F. Pinton[1,a]

[1] Laboratoire de Physique de l'École Normale Supérieure de Lyon, CNRS and Université de Lyon, 46 allée d'Italie, 69364 Lyon, France
[2] Laboratoire de Physique de la Matière Condensée et Nanostructures, CNRS and Université de Lyon, 43 boulevard du 11 Novembre 1918, 69622 Villeurbanne, France

Received 30 August 2007 / Received in final form 12 November 2007
Published online 16 January 2008 –

Abstract. We make time resolved velocity measurements of steel spheres in free fall through liquid using a continuous ultrasound technique. We explore two different ways to induce large changes in drag on the spheres: 1) a small quantity of viscoelastic polymer added to water and 2) altering the surface of the sphere. Low concentration polymer solutions and/or a pattern of grooves in the sphere surface induce an early drag crisis, which may reduce drag by more than 50% compared to smooth spheres in pure water. On the other hand, random surface roughness and/or high concentration polymer solutions reduce drag progressively and suppress the drag crisis. We also present a qualititative argument which ties the drag reduction observed in low concentration polymer solutions to the Weissenberg number and normal stress difference.

PACS. 47.85.lb Drag reduction – 47.32.Ff Separated flows – 47.63.mc High Reynolds number motions

1 Introduction

Reduction of drag in turbulent flows due to a small quantity of viscoelastic polymer added to the fluid has been the subject of intense research for more than 50 yrs (e.g. [1,2]). For example, the addition of as little as 5 parts per million (ppm) of polyacrylamide to turbulent pipe flow can result in an increase in flow speed of 80% for a given imposed pressure drop [3]. Similar flows with rough or structured wall surfaces have also been shown to exhibit reduction in drag (e.g. [4,5]). Our experiments address drag reduction by similar mechanisms for bluff bodies, which has received far less attention in spite of the potential impact on a broad range of phenomena and applications (aircraft, underwater vehicles and ballistics, predicting hail damage, sports ball aerodynamics, fuel pellets, etc.).

The aim of our work is to explore the influence of polymer additives in the fluid as well as sphere surface structure on the drag experienced by free falling spheres. Before we review the literature on these topics, let us first recall the main characteristics and terminology of high Reynolds number flow around spheres. (Reynolds number is defined as $Re = UD/\nu$ where U is sphere speed, D is sphere diameter, and ν is the kinematic viscosity of the fluid.) In the range $10^4 < Re < 10^7$, two basic phenomena are responsible for the most prominent flow features: flow separation and the transition to turbulence in the sphere boundary layer. For $200 < Re < Re_w^* \approx 3 \times 10^5$ flow separation occurs. (The w subscript distinguishes the value for smooth spheres in pure water from the different cases discussed later.) In this regime, laminar flow extends from the upstream stagnation point to slightly downstream of the flow separation point, i.e. the turbulence develops *downstream* from the separation point. In contrast, at Re just above Re_w^*, the boundary layer becomes turbulent *upstream* of the flow separation point. The resulting change in the velocity profile abruptly moves the separation point downstream. Since the drag on the sphere is dominated by pressure drag (form drag), this jump in the separation location results in a severe drop in drag, the so-called *drag crisis* [6–9]. In this range of Re, friction drag contributes not more than 12% to the total drag on a smooth sphere [6]. Although indirectly, our investigation is essentially exploring the effects of polymer additives and sphere surface structure on the dynamics of boundary layer separation and transition to turbulence.

We now briefly review studies which directly address these issues. Both Ruszczycky [10] and White [11] measured drag on a falling sphere in aqueous polymer solutions at $Re < Re_w^*$. Ruszczycky studied relatively high concentrations between 2500 and 15 000 ppm (by weight) of poly(ethylene oxide) (4×10^6 molecular weight (MW)) and guar gum (unknown MW) for a range of sphere sizes from 9.5 to 25.4 mm in diameter. Maximum drag reduction of 28% was found for a 25.4 mm sphere in 5000 ppm guar gum solution. For higher concentrations (15 000 ppm) the drag was found to increase compared to

[a] e-mail: pinton@ens-lyon.fr

water, probably because such high concentrations tend to be rather viscous. White used the same polymer at smaller concentrations with a similar range of sphere sizes and found a 45% maximum reduction in drag for a 75 ppm solution. White [12] and more recently Watanabe et al. [13] investigated a range of Re spanning the drag crisis. Their work suggests that at polymer concentrations above about 30 ppm, the drag crisis is replaced by a gradual decrease in drag which manifests as drag reduction for $Re < Re_w^*$ and drag enhancement for supercritical $Re > Re_w^*$. This is consistent with the observations of White and Ruszczycky below the drag crisis, as well as water tunnel measurements with circular cylinders [14]. At smaller polymer concentrations (5 to 10 ppm) the situation is less clear. A. White's measurements show erratic variation of drag as Re is increased, while Watanabe et al. report no change in behavior compared to water. Cylinder studies, in contrast, show a more sharply defined drag crisis at low polymer concentration [14]. One of the goals of our work is to better understand the nature of low concentration polymer effects near the drag crisis.

Concerning free falling rough spheres, to our knowledge, only one experimental work exists in the literature. In this short, qualitative study, White explored the combined effects of surface roughness and polymer additives [15]. He found that roughening the sphere surface shifts the wake separation point downstream, reducing drag, but with both a rough surface and polymers added the separation point shifts back upstream, increasing drag. Our observations add to White's intriguing results.

Wind tunnel measurements for both spheres [16] and cylinders [17] indicate that the drag crisis is shifted to lower Re when the surface is roughened. The roughened surface triggers an early transition to turbulence in the boundary layer. Golf balls are made with surface dimples in order to reduce drag by a very similar mechanism [18]. Furthermore, Maxworthy showed that adding a trip on the upstream surface of a smooth sphere induces a turbulent boundary layer and early drag crisis [8]. We are aware of no fixed sphere studies addressing roughness and polymer effects together. We add a note of caution to the reader that fixed (wind tunnel) and free-falling spheres may not behave the same. The first case corresponds to a fixed velocity of the upstream flow, while the second corresponds to a constant force driving the motion. Unlike the fixed sphere, a falling sphere cannot exist in a steady state with Re very close to Re_w^*; it is not a stable solution. Furthermore, even at terminal fall speed the wake is never truly steady. It is dynamically active with long-lived non-axisymmetric spatial structure. As a result, the "terminal" fall velocity of a sphere fluctuates in both direction and magnitude, which may lead to small discrepancies in comparing to wind tunnel data or to other free-fall experiments.

This paper is organized as follows. The next section presents the experimental procedures and equipment. In Section 3 we present our measurements for the free fall of smooth or roughened spheres in water and in solutions containing small polymer amounts. We discuss our results in terms of changes in drag with varying Reynolds number, polymer concentration and surface conditions. In the last section, we link our results at low polymer concentrations to the effects of a coil-stretch transition [27].

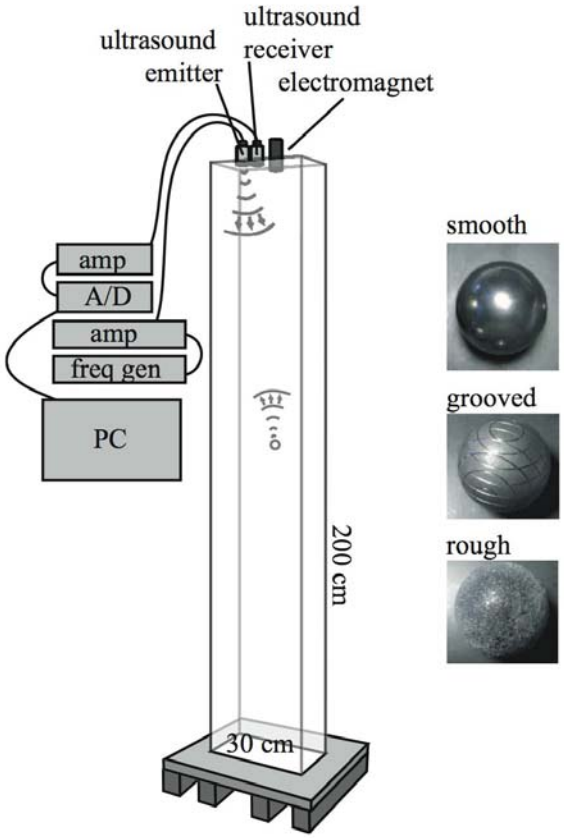

Fig. 1. Setup: the vertical velocity of falling steel spheres is measured with an ultrasound device. The fluid is tap water, pure or with small amounts of polymer additives. Smooth, grooved, and rough spheres are tested.

2 Measurement system and technique

We measure the fall velocity of steel spheres (ball bearings with density $\rho = 7.8$ g/cm^3) with diameters ranging from 3 mm to 80 mm. Two types of sphere surfaces are investigated in addition to the polished smooth surface (see photos in Fig. 1). The first type, grooved spheres, have have a regular pattern of grooves machined into the surface. The grooves are 500 μm deep, 1 mm wide. The second type corresponds to roughened surface, produced either by sanding the smooth polished spheres or by gluing onto the surface a single layer beads. In the first case, changes in the surface height are of the order of 10 microns. In the second case, we have used spherical glass beads 700 μm in diameter. The fluid vessel is 2 m tall and 30×30 cm in lateral dimension with walls made of 2 cm thick acrylic plate. The tank is filled with either tap water or a dilute aqueous solution of polyacrylamide (MW

5×10^6, granulated form, Sigma-Aldrich). The polymer solutions range in concentration between 5 and 200 ppm by weight. The polymers are mixed first with 2 liters of water with a magnetic stirrer for at least 8 h and then mixed with another 180 liters of water for 5 min in the experimental vessel. Tests with colored dye in the fluid confirm that this procedure effectively mixes the fluid. These polymer concentrations are in the dilute regime, significantly below the estimated overlap concentration of 1200 ppm. The Weissenberg number Wi, defined as the ratio of polymer relaxation time $\tau_R \sim 10^{-4}$s to flow time scale (see Sect. 4.2 for details), ranges between 0.8 and 2.3.

The spheres are released at the top of the vessel using an electromagnet. The speed of the ball is obtained using a continuous ultrasound technique. This technique is described in more detail in previous publications [20,21], and we briefly recall it here. One ultrasound transducer positioned at the top of the vessel emits sound at 2.8 MHz into the fluid. As the sphere falls it scatters sound at a Doppler shifted frequency which is measured with a second ultrasound transducer located near the emitter. The recorded signal is processed to recover the vertical component of the sphere velocity. The processing entails mixing the recorded signal with a 2.8 MHz sinusoid, low pass filtering, decimating to a lower sample rate, and finally using a parametric time-frequency analysis algorithm (MVA, see Ref. [21]) to recover the time varying Doppler shifted frequency. The resulting absolute precision for the velocity measurement is about 2 cm/s with a relative precision in mm/s. With typical fall speeds of several m/s, this is better than 1% precision. At such high Reynolds numbers (10^4–10^6), the flow in the wake contains significant non-axisymmetric flow structures [7], which often cause some lateral motion of the sphere. We present data only from trajectories that remained at least one sphere diameter away from the vessel walls throughout the fall. Based on studies of tunnel blockage effects for fixed spheres, we expect that walls have less than 5% influence on measured drag coefficients [16]. Furthermore, any wall influence is similar for the different polymer solutions and sphere surfaces allowing for meaningful *comparisons* between the different cases.

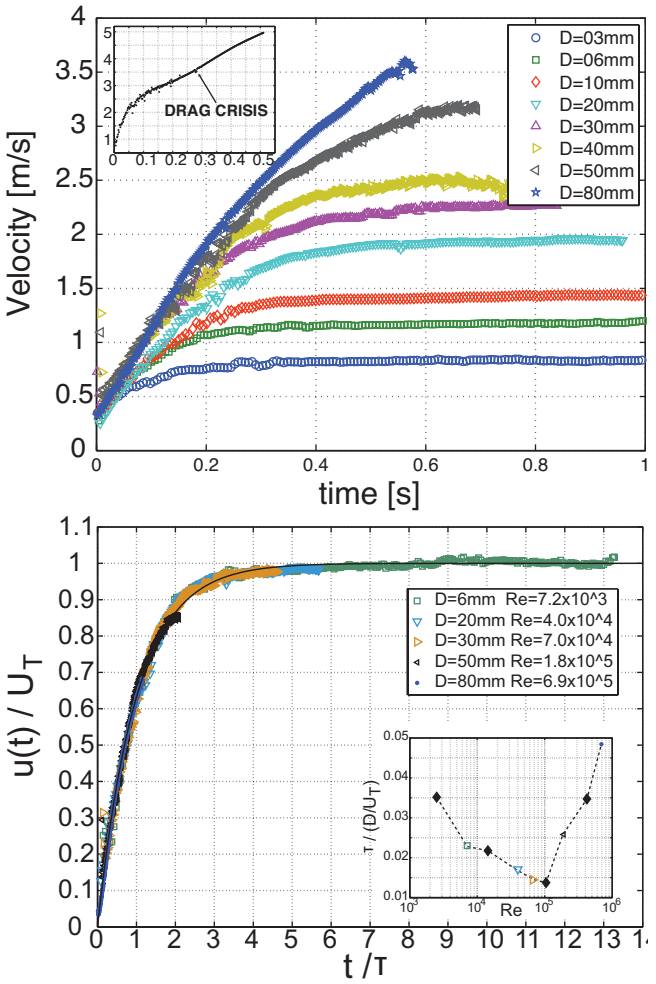

Fig. 2. Water and smooth spheres: (a) Time series of the spheres vertical velocity $u(t)$ during their free fall. The inset shows the drop – with a non zero initial velocity – of a 60 mm sphere: as its velocity reaches 3.5 m/s it experiences the drag crisis. (b) Comparison of the experimental data with a model $u(t) = U_T(1 - \exp(-t/\tau))$ exponential evolution. The parameters (τ, U_T) are obtained using a multidimensional unconstrained nonlinear minimization (Nelder-Mead) with MATLAB. The inset shows the evolution of the characteristic time τ with the Reynolds number. Note the sharp change in behavior near the drag crisis.

3 Experimental results

In this section, we present our observations in the form of either drag coefficient estimates or velocity time series. Each presented measurement is the result of averaging over several trajectories under the same conditions. We find that each drop is reproducible up to instantaneous differences up to several percent. We first discuss our measurements of smooth spheres falling in water, which provide a baseline for comparisons to the results from our experiments with polymer solutions and rough spheres. Next, we present measurements of smooth sphere behavior in polymer solutions. Then we explore the consequences of surface grooves or roughness in water. And finally, we address the combined case of altered-surface spheres in polymer solutions.

3.1 Water

We show in Figure 2a the fall velocity time series for the spheres with diameter D varying between 3 mm and 80 mm. As the spheres are released from rest, they accelerate until a terminal velocity U_T is reached – although for the larger spheres the water tank is not sufficiently tall for this steady state to be reached. The dynamics at the onset of motion is quite complex. Added mass effects, as well as wake-induced lift forces and history forces play a role [19,20]. However when the Reynolds number is large the dominant forces at work during the vertical fall of the sphere are the gravitational force $F_B = 1/6(\rho_S - \rho_F)\pi D^3 g$ and an effective drag force $F_D = 1/8 C_D \pi \rho_F D^2 U_T^2$, where

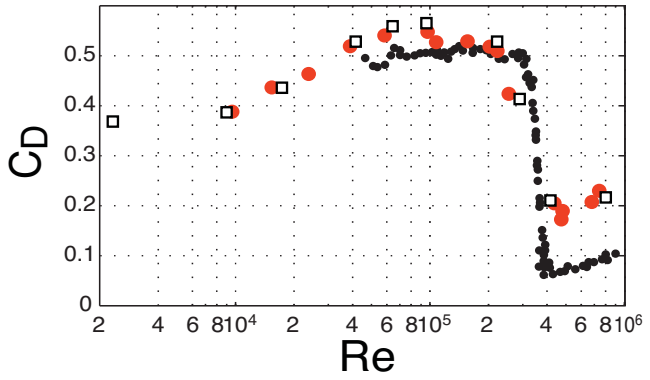

Fig. 3. Drag coefficient measurements for smooth spheres in water. Large red circles – our data; small black circles – Achenbach (wind tunnel) [16]; open squares – White's data [12].

C_D is the usual drag coefficient; ρ_F and ρ_S are the fluid and sphere densities. In the steady state, these forces balance and one may then compute the drag coefficient as

$$C_D = \frac{4}{3}\frac{(\rho_S/\rho_F - 1)Dg}{U_T^2}. \quad (1)$$

We note here that, unlike wind tunnel experiments, the velocity is not prescribed so that both C_D and Re are empirically computed from the data – the equation above may be viewed as an implicit relationship for $C_D(Re)Re^2$ as a function of the control parameters of the experiment.

We observe that during the approach to terminal speed, the trajectories for different sphere sizes are fully characterized by one time scale τ and the terminal speed U_T. We may extract τ and U_T from each velocity time series by fitting the data to an exponential of the form, $u(t) = U_T(1-e^{-t/\tau})$. In agreement with previous observations [20], the exponential is simply an effective tool used to extract τ and U_T and does not accurately represent the more complex dynamics of the true trajectory. When scaled by τ and U_T, all the time series in Figure 2a collapse onto one curve, verifying the importance of these two characteristic quantities. Using the exponential fit on the entire time series, we take advantage of our good resolution in both time and velocity magnitude to obtain accurate measurements of U_T even though the fall distance is only 2 m. Since this method integrates the whole time record of the fall, it also avoids possible errors incurred by taking single point measurements as has been done in past studies. Furthermore, inspection of the entire velocity time series is often very instructive, clearly revealing the drag crisis in some cases – see for instance the inset of Figure 2a, where a 60 mm sphere is shown to accelerate again as its Reynolds number exceeds Re_w^*.

We compare in Figure 3 our measurements of drag coefficients for smooth spheres in water to the free fall measurements of White [12] as well as the wind tunnel measurements of Achenbach [6]. We find an excellent agreement with White's data. In particular, we find that the critical Reynolds for the drag crisis is $Re_w^* = 2.8\times10^5$, a value that serves as a reference for comparison with the

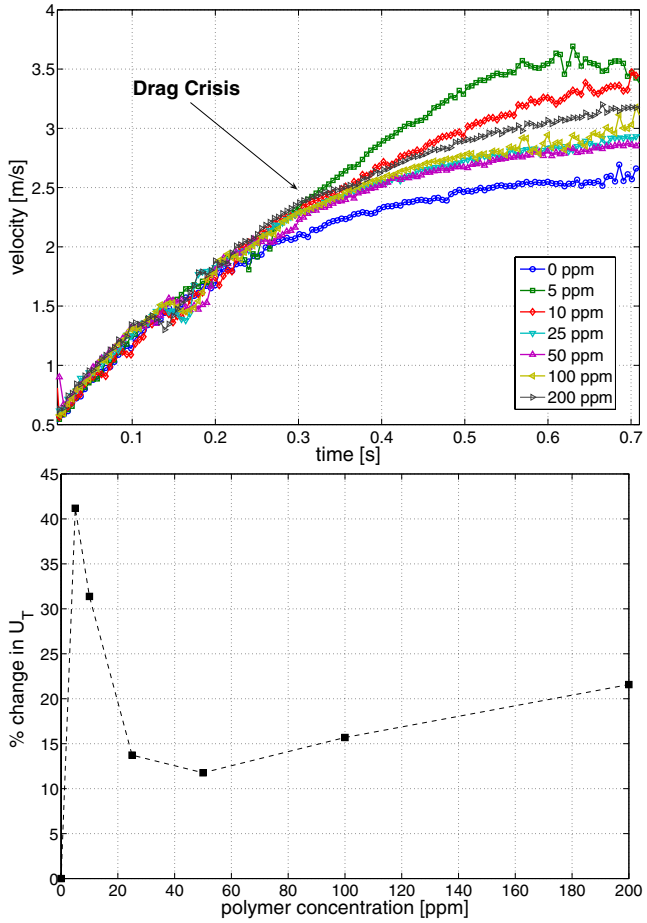

Fig. 4. Polymers: (a) Fall velocity time series of a 40 mm sphere in water, and polymer solutions with concentration increasing from 5 to 200 ppm. In the 5 and 10 ppm solutions the sphere undergoes a drag crisis where none existed for the pure water case. (b) Percentage change of terminal velocity U_T for increasing polymer concentration compared to pure water case for 40 mm sphere.

fall of spheres with modified surfaces and in water with additives. We also note that both White's data and ours suggest that the value of the drag coefficient just after the drag crisis for the free fall of spheres (imposed force case) is twice that observed in wind tunnel experiments (imposed velocity case).

3.2 Polymer solution

We first present velocity time series for a 40 mm sphere falling in a range of polymer concentrations in Figure 4a. We observe that at all concentrations the sphere terminal velocity is larger than in pure water; drag is reduced. This effect is greatest at small polymer concentrations, as demonstrated in Figure 4b: drag reductions over 30% have been observed for polymer concentration less than 20 ppm, while at higher concentrations the change is 10–25%. In the 5 and 10 ppm solutions, one observes a sudden acceleration of the sphere once it achieves a velocity

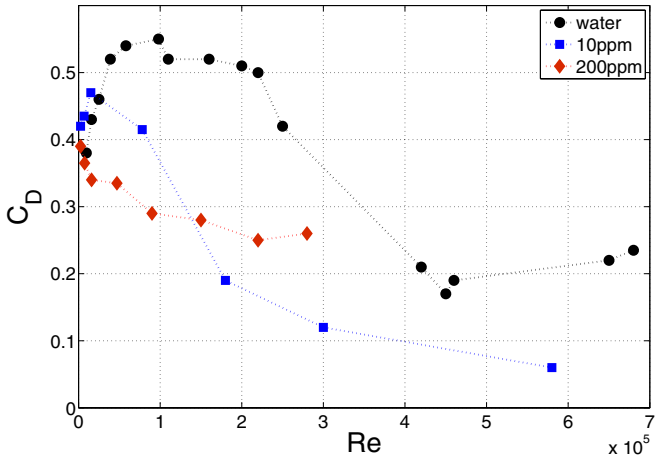

Fig. 5. Polymers: Drag coefficient measurements for smooth sheres in water (circles) compared to polymer solution. In 10 ppm solution (squares) the drag crisis is shifted to lower Re. In 200 ppm solution (diamonds) the drag crisis is replaced by a gradual decrease in drag.

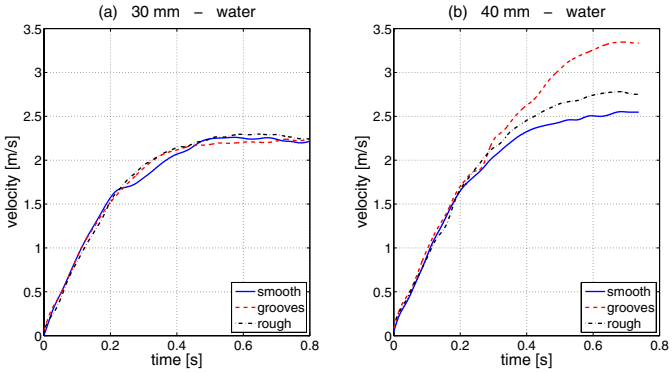

Fig. 6. Rough and grooved spheres: velocity time series for grooved (dashed line) and rough spheres (dash-dotted line) compared to smooth spheres (solid line) in pure water. The grooved surface induces an early drag crisis.

of about 2.5 m/s; this is the drag crisis. Examining the data for a range of sphere sizes in the 10 ppm solution (see Fig. 5a), we see that the critical Reynolds number is then $Re^*_{polymer} \sim 1.0 \times 10^5$, almost a third of the value $Re^*_w \sim 2.8 \times 10^5$ in pure water. On the other hand, at higher polymer concentrations, we do not observe a jump in the velocity time series and their is no discontinuity in the drag $C_D(Re)$ curve. One observes that for high polymer concentrations, compared to the low concentration case, the drag is reduced at $Re < Re^*_{polymer}$, but enhanced for $Re > Re^*_{polymer}$. This data suggests that there is no drag crisis for high polymer concentrations, but instead the drag decreases continuously with increasing Re. These observations are consistent with the experiments of previous investigations using poly(ethylene oxide) in a similar range of concentrations [12,13]. We have not been able to reach Reynolds numbers high enough to determine whether the drag would reach a common asymptotic limit.

3.3 Rough and grooved surfaces in water

In exploring surface structure effects, we concentrate our attention on 30 and 40 mm spheres, whose Re in pure water lies just below the drag crisis. The time series in Figure 6 illustrate the different behaviors for the different surfaces we studied. In pure water, both the 30 mm grooved sphere and rough sphere behaves the same as the 30 mm smooth sphere — cf. Figure 6a. In contrast, adding grooves to the 40 mm sphere induces a drag crisis, as shown in Figure 6b. The 40 mm rough sphere showed moderate drag reduction, but not a well defined crisis. Indeed, the dynamics in Figure 6b shows that the terminal velocity is increased compared to the smooth sphere, but there is no clear change in the acceleration as in the case of the grooved sphere.

Grooves are thus able to shift the drag crisis from $Re^*_w \sim 2.8 \times 10^5$ to $Re^*_{grooves} \sim 0.8 \times 10^5$. In the case of the 40 mm sphere, the terminal velocity increases from 2.5 m/s to 3.4 m/s, corresponding to a drag reduction of 46%. For the rough sphere, a drag reduction is also observed but it is limited to a 20% gain. This difference in behavior is not yet understood. One may note that a rough surface destabilizes the boundary layer but also increases friction and dissipation.

Finally, we have observed that sanded spheres (rugosity of the order of 10 μm) with a diamater of 30 and 40 mm showed no change compared to smooth spheres. This indicates that surfaces modifications must exceed the thickness of the viscous sub-layer in order to produced measurable effects on the dynamics.

3.4 Rough and grooved surfaces in polymer solution

We now examine the changes in the above described behavior when polymer is added to the water. We find that the two regimes of low and high concentration – Section 3.2 – are affected differently by adding grooves to the sphere surface. Results for the grooved spheres are presented in Figure 7. At low concentration the shift of the drag crisis to lower Re due to polymer is exaggerated by adding grooves to the sphere; Re^*_w is shifted even lower. Indeed, in a 5 ppm solution, the 30 mm grooved sphere experiences the drag crisis, whereas the same sphere in water as well as the smooth 30 mm sphere in 5 ppm solution do not. We find that the $Re^*_{grooved+poly} \sim 6 \times 10^4$, a further gain of 20% compared to polymers alone. At higher polymer concentration, the spheres behave identically with or without grooves.

The rough sphere did not exhibit the same behavior. Rather, the surface roughness seems to suppress the drag crisis, in agreement with the observations of White [15]. Our results are presented in Figure 8, for a 40 mm sphere. When the surface is smooth, one observes as before the shift in the drag crisis and a very large terminal velocity

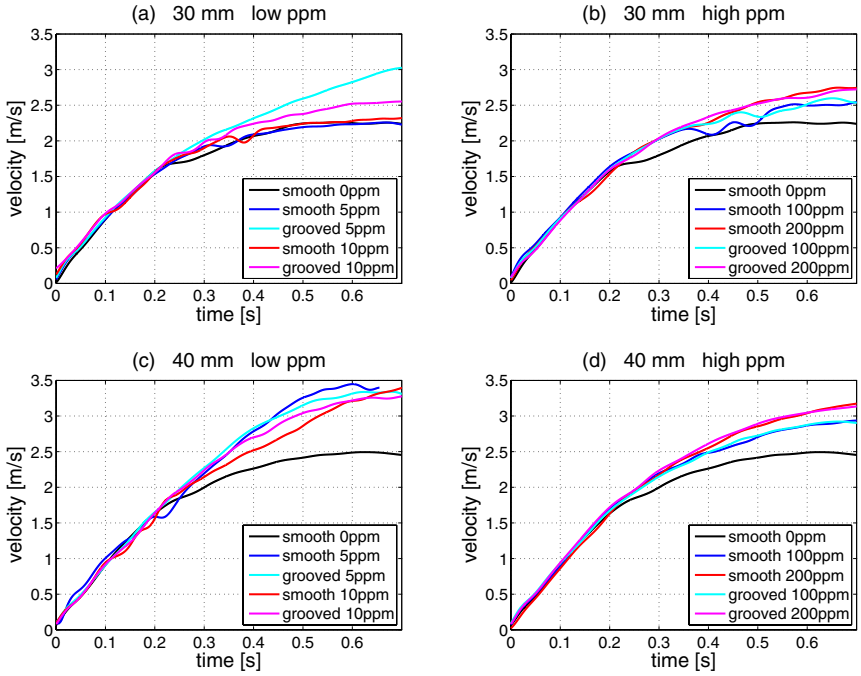

Fig. 7. Grooved spheres and polymers: At low polymer concentration (left column) adding grooves to the sphere induces an even earlier drag crisis compared to the smooth sphere. At high concentration (right column) grooves do not change the observed dynamics.

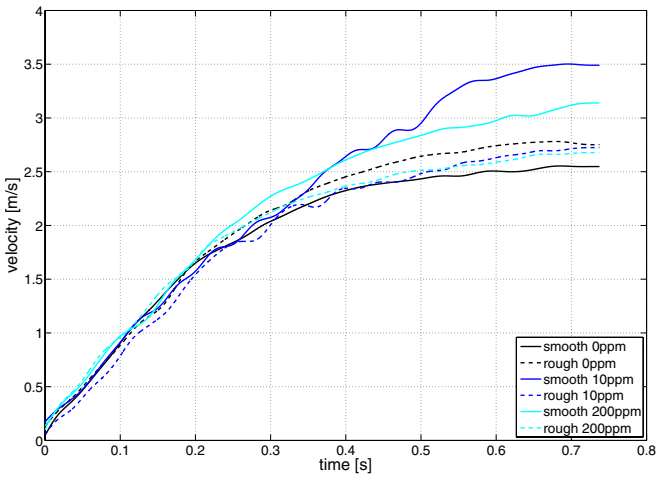

Fig. 8. Rough sphere (40mm): Adding polymer causes nearly no change in the behavior of rough spheres, and suppresses the drag crisis independent of the polymer concentration.

at low polymer concentration (10 ppm), as well as a reduced drag at high concentration (200 ppm). However, for the rough sphere all dynamical $v(t)$ curves are very close. The rough spheres experience no further decrease in drag in the polymer solutions, compared to what is already induced by the surface roughness. In fact, there even may be a slight increase in drag (of the order of 5%) when the rough sphere falls in the water and polymer solution, at any concentration.

4 Discussion

4.1 Experimental summary

We have conducted a series of experiments using precise and time resolved ultrasound velocity measurements to compare the behavior of rough and smooth steel spheres falling through water or dilute aqueous polymer solutions. Remarkably, we find that in low concentration polymer solutions (5 to 20 ppm) the drag crisis happens at a lower Reynolds number than in water. By adding a pattern of shallow grooves to the sphere surface, we shift the drag crisis to even lower Re. Adding grooves to a sphere in pure water also shifts the drag crisis to lower Re. On the other hand, a sphere roughened with a layer of 700 μm beads glued to its surface never experiences a drag crisis, exhibiting nearly the same drag with or without polymers. The drag on a rough sphere is slightly less than that on a smooth sphere. For higher concentration polymer solutions (100–200 ppm) and smooth spheres the drag crisis is suppressed and replaced by a more gradual decrease in drag as Re is increased. This high concentration behavior is largely unchanged by adding grooves to the sphere surface.

Our measurements seem to indicate that for low concentrations the polymers are able to induce the transition to turbulence but have little effect on the location of flow separation whether laminar or turbulent. That is, low polymer concentrations induce an early drag crisis, but do not greatly change the drag before and after the crisis, so that we may conclude that the location of the

separation points have not been significantly changed. In fact, we have observed that the dynamical behavior $v(t)$ is quite well modelled by a simple shift in the $C_D(Re)$ curve, coupled to a simple dynamical equation in which only the drag force is accounted for. Compared to low polymer concentration we find that at high concentration drag is reduced at low Re and enhanced at higher Re.

Surface roughness is commonly understood to induce an early transition to boundary layer turbulence [8], which may explain the shift in Re_w^* observed for the grooved sphere. On the other hand, it is difficult to explain in the same context our observation of rather weak drag reduction and apparent suppression of the drag crisis for the rough sphere. Perhaps friction drag is significant in this case. Further investigation of this curious behavior is left for future work.

4.2 Drag crisis and normal stress difference

In this section we try to rationalize the effect of the polymers on the observed drag reduction. We follow ideas proposed for drag reduction in pipes [25] and much developed since (see for instance [28]). Specifically, a change of conformation of the polymer is argued to be the source of the modification of the drag crisis.

As discussed above, the drag crisis is the result of the destabilization of the laminar boundary layer [23]. At a critical Reynolds number the boundary layer becomes turbulent, shifting the separation line downstream and reducing accordingly the drag on the sphere. The polymer has *a priori* little effect on the parameters influencing this boundary layer transition, like the viscosity η. Indeed the polymer concentration is smaller than the overlap concentration $\xi^\star$, separating the dilute from the semi-dilute regime [24] – for the polymers under consideration, this is estimated to be $\xi^\star \simeq 1200$ ppm. The shear viscosity of the polymer solutions in water, η_P, is related to the polymer density according to $\eta_P = \eta_w(1 + 1.49\xi/\xi^\star)$ with η_w the water viscosity [24]. Thus for the low concentrations under consideration here, $\xi \ll \xi^\star$, the viscosity is close to that of water $\eta \sim \eta_w$.

However this estimate assumes that the polymers' structure is not affected by the flow. Velocity gradients may locally induce a stretching of the polymer, which can be quantified by the Weissenberg number defined as $Wi = \dot{\gamma}\tau_R$, with $\dot{\gamma}$ a deformation rate and τ_R the polymer relaxation time. Typically, for $Wi < 1$ the polymer is in a coil state, while for $Wi > 1$ stretching occurs. Let us estimate Wi in our geometry. The relaxation time is typically $\tau_R \sim \eta_w R_g^3/k_BT$, with R_g the radius of gyration of the polymer, $R_g \sim bN^{\nu_F}$ (b the monomer size and $\nu_F \simeq 3/5$ the Flory exponent). For the polymers under investigation, $\tau_R \sim 10^{-4}$ s. On the other hand the deformation rate is estimated as the shear rate in the boundary layer, i.e. $\dot{\gamma} \sim U/\delta$, with U the sphere velocity and $\delta \sim \sqrt{\nu D/U}$ the typical thickness of the boundary layer

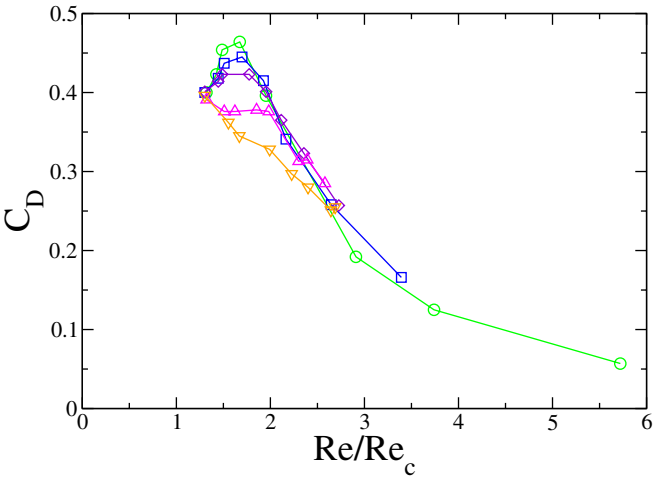

Fig. 9. Drag coefficient versus the reduced Reynolds number Re/Re_c. The different symbols correspond to various concentrations of polymers: (○) 10ppm; (square) 25ppm; (◇) 50ppm; (△) 100ppm; (▽) 200ppm. Lines are a guide to the eye. For a given polymer concentration, the different experimental points correspond to different size of the falling sphere (from left to right, $D = 3, 6, 10, 20, 30, 40, 50, 60$ mm).

(a the diameter of the sphere). This gives

$$Wi \sim \frac{U^{3/2}\tau_R}{\sqrt{\nu D}}, \tag{2}$$

which can be rewritten

$$Wi \sim \left(\frac{Re}{Re_c}\right)^{3/2}, \tag{3}$$

with a critical Reynolds number Re_c defined as

$$Re_c = \left(\frac{D^2}{\nu\tau_R}\right)^{2/3}. \tag{4}$$

At Re_c the polymer is thus expected to undergo – within the boundary layer - a coil-stretched transition and the drag will be accordingly be affected (as we discuss hereafter). This point is confirmed experimentally in Figure 9 where the drag coefficient is plotted versus the reduced Reynolds number Re/Re_c: the 'drag-crisis' is always found to occur for $Re \sim Re_c$ for the different cases investigated. While a full rescaling is not expected in this plot, this figure points to the relevance of the Weissenberg number as a key parameter to the polymer induced drag crisis: it does show that the drag crisis transition with polymers, i.e. when the drag coefficient strongly decreases, occurs at a Reynolds number of the order of the critical Reynolds number, $Re \sim Re_c$. This indicates that the drag crisis criterion with polymers corresponds to $Wi \sim 1$, as also observed in earlier works.

At this level, the previous discussion suggests that the polymer effect on the drag crisis is associated with a conformation change. The question of the polymer-flow coupling however remains, and in particular the origin of an earlier destabilization of the boundary layer.

First, as the polymers in the boundary layer become stretched, most of the properties of the polymer solution in this region will change dramatically: the typical size of the polymer increases indeed from the radius of gyration to the much larger contour length of the polymer, $L \gg R_g$. This affects the relaxation time which now becomes $\tau_R \sim \eta_w L^3/k_B T$, and therefore the viscosity which increases typically by a factor $(L/R_g)^3 = N^{3(1-\nu_F)} \gg 1$. However, increasing the viscosity in the boundary layer amounts to a *decrease* in the local Reynolds number: this would lead to a re-stabilization of the laminar boundary layer, an effect which is opposite to the experimental observation.

Another origin has therefore to be found. We suggest that the destabilization of the boundary layer originates in a very large *normal stress difference* occurring when the polymer is in its strechted state. Normal stress difference is a non-Newtonian effect which is commonly observed in polymer solutions [24]. This is known to lead for example to the Weissenberg (rod-climbing) effect. In our geometry, the normal stress difference is expected to be proportional to the square of the shear-rate according to

$$\Delta\sigma = \sigma_{xx} - \sigma_{yy} = \Psi_P \dot{\gamma}^2 \tag{5}$$

with Ψ_P a transport coefficient ; σ_{xx}, σ_{yy} are the normal components of the stress tensor in the x and y directions, with $\{x, y\}$ local coordinates respectively parallel and perpendicular to the sphere surface (curvature effects are neglected).

Let us show that this term does destabilize the boundary layer. Classically, the boundary layer is destabilized by a *negative* pressure gradient term due to a decrease of the fluid velocity $U_e(x)$ in the outer layer [23]: $-\nabla P_e = \rho U_e(x) \nabla U_e(x)$, with $U_e(x)$ the fluid velocity outside the boundary layer. A stability analysis of the boundary layer with such a pressure gradient leads to a destabilization at a reduced Reynolds number [23] $Re_\delta = U\delta/\nu \sim 600$, corresponding to $Re \sim 10^5$. The normal stress difference adds a contribution to this term, leading to an supplementary effective pressure gradient term

$$-\nabla P_{\text{eff}} = \rho U_e(x) \nabla U_e(x) + \Psi_P \nabla \dot{\gamma}^2, \tag{6}$$

where $\dot{\gamma} \simeq U_e(x)/\delta(x)$ and $\delta(x) \simeq \sqrt{\nu x/U_e(x)}$ the local thickness of the boundary layer. It is easy to verify that this supplementary contribution to the effective pressure gradient will be negative - and therefore destabilizing, *before* the classical contribution $\rho U_e(x) \nabla U_e(x)$. Moreover in the stretched state ($Wi > 1$), one may verify that this contribution is dominant as compared to the classical one. The ratio Δ between these two terms is of order $\Delta \sim \Psi_P \dot{\gamma}^2/\rho U_e^2$. Using $\Psi_P \sim \eta_P \tau_P$ with η_P the polymer contribution to the viscosity and τ_P the polymer relaxation time [24], one deduces $\Delta \sim U\tau_P/D \sim (L/R_g)^3/\sqrt{Re_c}$ (for $Re = Re_c$). In our case, with $Re_c \sim 10^5$, $(L/R_g)^3 = N^{3(1-\nu_F)} \sim 2 \times 10^5$ ($N \simeq 35 \times 10^3$), one has $\Delta \sim 10^3 \gg 1$. This term thus leads to a strong destabilization as soon as the polymer is stretched.

To summarize, for $Re \geq Re_c$ the coil-stretched transition occurs for the polymer in the boundary layer, and the existence of a normal stress difference induces a strong destabilization of the laminar boundary layer. This scenario gives the trends of the underlying mechanisms leading to a shift of the drag crisis even for very small amounts of polymers. For the polymer additive to have an effect, the critical Reynolds number has to be *lower* than the critical Reynolds number for the drag crisis in pure water, $Re_w^\star$: $Re_c = \left(\frac{D^2}{\nu \tau_R}\right)^{2/3} < Re_w^\star$. This provides a condition in terms of the size of the falling object but also a minimal polymer weight (since $\tau_R \propto N^{3\nu}$). To go further, a more detailed stability analysis of the boundary layer with the supplementary normal stress difference is needed. We leave this point for further studies.

References

1. J.L. Lumley, Ann. Rev. Fluid Mech. **1**, 367 (1969)
2. N.S. Berman, Ann. Rev. Fluid Mech. **10**, 47 (1978)
3. B.A. Toms, *Proc. Int. Congress. Rheology Amsterdam*, Vol. 2 (North-Holland, Amsterdam 1949) p. 135
4. M. Vlachogiannis, T.J. Hanratty, Exp. Fluids **36**, 685 (2004)
5. H.L. Petrie, S. Deutsch, T.A. Brungart, A.A. Fontaine, Exp. Fluids **35**, 8 (2003)
6. E. Achenbach, J. Fluid Mech. **54**, 565 (1972)
7. S. Taneda, J. Fluid Mech. **85**, 187 (1978)
8. T. Maxworthy, Trans. ASME, J. App. Mech. **36**, 598 (1969)
9. G. Constantinescu, K. Squires, Phys. Fluids **16**, 1449 (2004)
10. M.A. Ruszczycky, Nature **206**, 614 (1965)
11. D.A. White, Nature **212**, 277 (1966)
12. A. White, Nature **216**, 995 (1967)
13. K. Watanabe, H. Kui, I. Motosu, Rheol. Acta **37**, 328 (1998)
14. T. Sarpkaya, P.G. Rainey, R.E. Kell, J. Fluid Mech. **57**, 177 (1973)
15. A. White, Nature **211**, 1390 (1966)
16. E. Achenbach, J. Fluid Mech. **65**, (1974) 113
17. Y. Nakamura, Y. Tononari, J. Fluid Mech. **123**, 363 (1982)
18. J. Choi, W.-P. Jeon, H. Choi, Phys. Fluids **18**, 041702 (2006)
19. M.R. Maxey, J.J. Riley, Phys. Fluids **26**, 883 (1983)
20. N. Mordant, J.-F. Pinton, Eur. Phys. J. B **18**, 343 (2000)
21. N. Mordant, P. Metz, O. Michel, J.-F. Pinton, Rev. Sci. Instr. **76**, 025105 (2005)
22. A. Acharya, R.A. Mashkelhar, J. Ulbrecht, Rheol. Acta, **15**, 471 (1976)
23. H. Schlichting, Boundary layer theory (Mac-Graw Hill, New York, 1968)
24. M. Doi, S. Edwards, The theory of polymer dynamics (Clarendon press, Oxford, 1986)
25. J.L. Lumley, Symp. Math. **9**, 315 (1972); J.L. Lumley, J. Polym. Sci., Part D: Macromol. Rev. **7**, 263 (1973)
26. E. Balkovsky, A. Fouxon, V. Lebedev, Phys. Rev. Lett. **84**, 4765 (2000)
27. P.G. deGennes, J. Chem. Phys. **60**, 5030 (1974)
28. K.R. Sreenivasan, C.M. White, J. Fluid Mech. **409**, 149 (2000); R. Benzi, V.S. L'vov, I. Procaccia, V. Tiberkevich, Europhys. Lett. **68**, 825 (2004); A. Celani, S. Musacchio, D. Vincenzi, J. Stat. Phys. **118**, 531 (2005)